

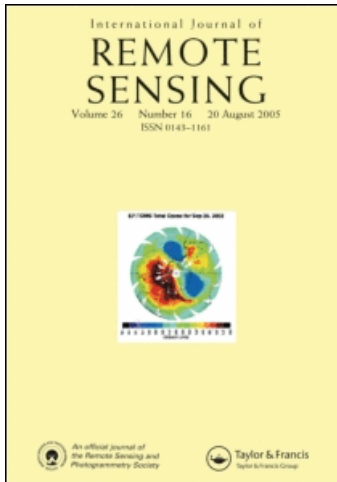
This article was downloaded by: [University of Tokyo/TOKYO DAIGAKU]

On: 20 August 2008

Access details: Access Details: [subscription number 778576937]

Publisher Taylor & Francis

Informa Ltd Registered in England and Wales Registered Number: 1072954 Registered office: Mortimer House, 37-41 Mortimer Street, London W1T 3JH, UK



## International Journal of Remote Sensing

Publication details, including instructions for authors and subscription information:

<http://www.informaworld.com/smpp/title-content=t113722504>

### Accuracy and applicability of linear spectral unmixing in delineating potential erosion areas in tropical watersheds

A. M. de Asis<sup>a</sup>; K. Omasa<sup>a</sup>; K. Oki<sup>a</sup>; Y. Shimizu<sup>a</sup>

<sup>a</sup> Graduate School of Agricultural and Life Sciences, The University of Tokyo, 1-1-1 Yayoi, Bunkyo-ku, Japan

Online Publication Date: 01 January 2008

**To cite this Article** de Asis, A. M., Omasa, K., Oki, K. and Shimizu, Y. (2008) 'Accuracy and applicability of linear spectral unmixing in delineating potential erosion areas in tropical watersheds', *International Journal of Remote Sensing*, 29:14, 4151 — 4171

**To link to this Article:** DOI: 10.1080/01431160701874579

**URL:** <http://dx.doi.org/10.1080/01431160701874579>

PLEASE SCROLL DOWN FOR ARTICLE

Full terms and conditions of use: <http://www.informaworld.com/terms-and-conditions-of-access.pdf>

This article may be used for research, teaching and private study purposes. Any substantial or systematic reproduction, re-distribution, re-selling, loan or sub-licensing, systematic supply or distribution in any form to anyone is expressly forbidden.

The publisher does not give any warranty express or implied or make any representation that the contents will be complete or accurate or up to date. The accuracy of any instructions, formulae and drug doses should be independently verified with primary sources. The publisher shall not be liable for any loss, actions, claims, proceedings, demand or costs or damages whatsoever or howsoever caused arising directly or indirectly in connection with or arising out of the use of this material.

## Accuracy and applicability of linear spectral unmixing in delineating potential erosion areas in tropical watersheds

A. M. DE ASIS, K. OMASA\*, K. OKI and Y. SHIMIZU

Graduate School of Agricultural and Life Sciences, The University of Tokyo, 1-1-1  
Yayoi, Bunkyo-ku, Tokyo, 113-8657, Japan

(Received 22 February 2007; in final form 10 December 2007)

This study was undertaken to assess the accuracy of linear spectral unmixing (LSU) in estimating fractional abundance of land cover components and to examine its applicability in delineating potential erosion areas in tropical watershed. Five image end-members (mixed vegetation, grass, *Acacia auriculi-formis*, bare soil and water/shadow) were selected and used in different combinations in unmixing Landsat Enhanced Thematic Mapper (ETM) into fraction images. The accuracy assessment was conducted by comparing the land cover abundance estimates derived from unmixing with the land cover abundance measured from field-validated classified QuickBird imagery. Good agreement was obtained using a four-end-member combination in which shadow was eliminated. The results suggest that LSU could be implemented for soil erosion detection. In general, soil erosion increases when vegetation cover decreases; hence, we used the fraction images to derive a bare soil/vegetation cover ratio and used that as a simple indicator to map high potential erosion areas. Comparison with field assessment of actual erosion levels in the study area showed that the technique is effective in identifying areas on which erosion control efforts should be concentrated.

### 1. Introduction

Soil erosion is one of the most serious environmental problems in many parts of the world. In the Philippines, for instance, it is widely agreed that unless the rate of soil erosion is dramatically reduced, the country will continue to face severe degradation of water and soil resources. Erosion rates in the Philippines range from about  $1 \text{ t ha}^{-1} \text{ year}^{-1}$  in undisturbed forests to around  $300\text{--}400 \text{ t ha}^{-1} \text{ year}^{-1}$  in overgrazed or frequently burned grasslands, while the sediment discharges of rivers whose catchments are subject to uncontrolled manipulations exceed  $30 \text{ t ha}^{-1} \text{ year}^{-1}$  (David 1988). To undertake corrective measures and prevent further degradation of many watersheds, timely information on the extent and spatial distribution of erosion areas is of paramount importance. This information is necessary for cost-effective soil conservation planning.

Remote sensing has been used to identify and map erosion areas. These processes are usually accomplished by visual interpretation (Bocco *et al.* 1991, Kumar *et al.* 1996, Dwivedi *et al.* 1997, Fulajtar 2001) or by automatic extraction using unsupervised (Servenay and Prat 2003) and supervised (Bocco and Valenzuela 1988, Metternicht and Zinck 1998, Floras and Sgouras 1999) digital information

---

\*Corresponding author. Email: [omasa@mail.ecc.u-tokyo.ac.jp](mailto:omasa@mail.ecc.u-tokyo.ac.jp)

extraction. However, classification results of these techniques are very general and do not recognize or identify small areas, particularly if the resolution of the remote sensing data is low. The reflectance recorded within an image pixel may be a mixture of several surface components that cannot be detected by simple classification.

Consequently, a subpixel classification technique known as Spectral Mixture Analysis (SMA) has attracted increasing interest in soil erosion identification. SMA estimates fractional abundance of land cover components using end-members, which represent the spectral characteristics of land cover types. The Linear Spectral Unmixing (LSU) model (Adams *et al.* 1986, Smith *et al.* 1990, Sabol *et al.* 1992, Settle and Drake 1993, Van der Meer 1995, Small 2001, 2003, Wu and Murray 2003) is by far the most common type of SMA, and is widely used because of its simplicity and interpretability. It has been applied in mapping land degradation in semi-arid environments (Metternicht and Fermont 1998, Haboudane *et al.* 2002). However, despite its increasing widespread use, most LSU analyses do not validate the end-member fraction estimates they produce and relied only on the mathematical validity of the model. Attempts to validate the results of LSU are usually hindered by the difficulty of obtaining accurate measures of the abundance of land cover as projected into the image plane (Smith *et al.* 1990). Elmore *et al.* (2000) proposed a methodology based on point frame transect measurement of individual plants in a semi-arid environment but the procedure is very labour intensive and not appropriate for a tropical environment. In light of the current availability of so-called very high-resolution (VHR) images from IKONOS and QuickBird, better validation of fractional abundance estimates can be made. The high spatial resolution of the QuickBird sensor, in particular, allows it to image individual land cover components. Accordingly, if the fraction abundance estimates determined by SMA were similar to the fraction of surface components measured by QuickBird, the resulting agreement would provide better estimates on accuracy.

The objectives of this study were to assess the accuracy of LSU as applied to Landsat Enhanced Thematic Mapper (ETM) images, and to determine its applicability in mapping high potential erosion areas in tropical environment. The first part of the paper explains the analysis of spectral unmixing and its validation using field-validated classified QuickBird imagery. So far, there are no widely known studies that have made use of SMA in soil erosion mapping under tropical environments. Thus, the second part of the paper describes a methodology using the fraction images derived from spectral unmixing.

## 2. Study area and data used

### 2.1 Description of study area

The selected study area is the Lamesa watershed located in the northernmost part of Metro Manila, Philippines, between 14°43'1" to 14°48'46" N latitudes and 121°4'1" to 121°10'37" E longitudes (figure 1). The area covers about 7000 hectares and consists mainly of evergreen forests and grasslands. However, because of its proximity to an urban population, encroachment has made most of the area subject to high rates of land-use conversion. The recurring establishment and subsequent abandonment of agricultural lands that are often less than the size of a Landsat pixel (900 m<sup>2</sup>) has left many of the areas highly erodible. Some observable features are tracks of logged-over section, dirt roads, cultivated areas and patches of bare soils. A pixel of Landsat ETM could therefore be a mixture of these land cover features.

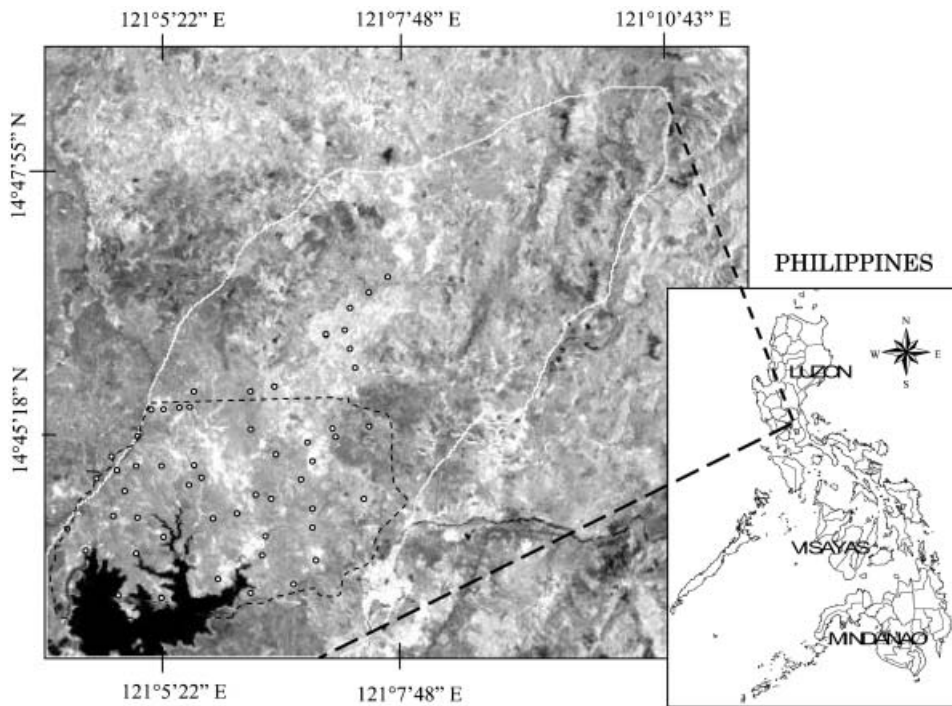


Figure 1. Geographic location of the study area. The dotted line represents the area with available QuickBird imagery, while the white dots show the relative locations of sampling sites.

For the purpose of soil conservation, monitoring and delineation of these areas are important for soil erosion assessment. Soil conservation is of significant concern because the watershed supports an important water resource of Metro Manila.

The topography of the Lamesa watershed is characterized by gently undulating terrain. The highest elevation is 248 m and the lowest is 64 m above sea level. Its climate is dominated by distinct rainy and dry seasons. It is relatively dry from December to April and wet from May to November with maximum monthly precipitation ranging from 488 to 1469 mm. Mean annual precipitation in the area is 2069 mm.

## 2.2 Satellite data

Two satellite images were used in this study, the Landsat 7 ETM+ (Landsat ETM) and QuickBird multispectral images, both acquired during the dry season in April 2004. The Landsat ETM (path 116/row 50) data were acquired on 24 April 2004 with the systematic correction (Level 1G) product (radiometrically corrected and geometrically corrected). The Landsat ETM has a temporal revisit time of 16 days and a spatial resolution of 30 m with six visible/near-infrared bands: band 1 (blue), 0.45–0.52  $\mu\text{m}$ ; band 2 (green), 0.52–0.60  $\mu\text{m}$ ; band 3 (red), 0.63–0.69; band 4 (near-infrared), 0.76–0.90  $\mu\text{m}$ ; band 5 (mid-infrared), 1.55–1.75  $\mu\text{m}$ ; and band 7 (mid infrared), 2.08–2.35  $\mu\text{m}$ . It also has one thermal (band 6, 10.40–12.50  $\mu\text{m}$ ) and a panchromatic band (band 8, 0.52–0.90  $\mu\text{m}$ ). In this study, the digital number (DN) of the image bands 1–5 and 7 recorded in 8 bits were converted to exoatmospheric (top-of-atmosphere) reflectance units as described in the *Landsat 7 User's Handbook*

(<http://landsathandbook.gsfc.nasa.gov/handbook.html>). These image bands were used in the analysis.

To assess the accuracy of the subpixel analysis used in this study, a QuickBird image with four multispectral bands [blue (0.45–0.52  $\mu\text{m}$ ), green (0.52–0.60  $\mu\text{m}$ ), red (0.63–0.69  $\mu\text{m}$ ) and near-infrared (0.76–0.90  $\mu\text{m}$ )] was used. The image was acquired on 25 April 2004, under clear sky conditions. The sun elevation at the time of capture was 67.2° with a close-to-nadir view angle of 14.8°. The imagery was referenced to the World Geodetic System 1984 (WGS84) datum and the Universal Transverse Mercator (UTM) coordinate system by the satellite data providers with an estimated published average absolute positional error of 23 m and a root mean square error (RMSE) of 14 m. To improve the positional accuracy, the imagery was orthorectified using the rational polynomial coefficients (RPCs), an additional set of ground control points (GCPs) collected with submetre accuracy differential global positioning system (DGPS) Magellan ProMark X-CM GPS receivers and a 4-m resolution digital elevation model (DEM) of the study area. The point accuracy of the orthorectified image with respect to GPS measurements was reduced to 2.20 m RMSE. Image DNs of QuickBird were also converted to exoatmospheric reflectance units using parameters provided by Digital Globe and following the procedure described in the *Landsat 7 User's Handbook*.

### 2.3 Image-to-image registration

After orthorectifying the QuickBird image, an image-to-image registration was performed between QuickBird and Landsat ETM, where the former was used as the reference image. Spatial registration was performed using manual control point extraction. In the process, 103 GCPs were collected on road intersections, edges and confluence of rivers. Terrain contour matching (Eugenio and Marquez 2003) was also performed to select accurate GCPs. The image was warped using a second-degree polynomial with nearest neighbourhood resampling. The resulting RMS error was equal to 0.21 pixel.

### 2.4 Field data

Fieldwork was conducted 1 month after the images were taken on 20, 21, 23 and 24 May 2004. The fieldwork basically involved the collection of ground truth data for the validation of the satellite images and establishment of validation/sampling sites. Prior to the field survey, both satellite images were interpreted and examined to obtain an overall view of the area. Sampling sites were systematically identified from both images and spatially registered using differentially corrected GPS.

Fifty-three sampling sites measuring 30 m  $\times$  30 m each were established in the study area (see figure 1). Through visual estimation, each sampling site was characterized in terms of its cover type and vegetation density. Actual ground cover abundance (e.g. mixed vegetation, grass, *Acacia auriculiformis*, bare soil) was determined from QuickBird in relation to ground observations. Actual soil erosion at each sampling site was also assessed. Four levels of soil erosion were defined according to the apparent soil erosion indicators such as vegetation amount, presence of rills or gullies, exposed subsoil and exposure of tree roots. The soil erosion levels were: erosion level 4 (severe erosion); erosion level 3 (high erosion); erosion level 2 (moderate erosion); and erosion level 1 (no erosion). Areas with erosion level 4 are characterized by severe erosion with very sparse vegetation,

exposed subsoil and the presence of deep channels and gullies. Areas that were mostly abandoned cultivated lands and staggered bare soil having visible rills/small channels and loss of topsoil were classified as erosion level 3. Grass-covered areas with newly growing trees (i.e. mostly *Acacia auriculiformis*) where soil erosion was not considerable were classified as erosion level 2. Finally, densely vegetated areas where no soil erosion could be observed were categorized as erosion level 1.

### 3. Methods

#### 3.1 High-resolution image classification

Figure 2 illustrates the method of analysis performed in this study. After georeferencing the two images, the QuickBird image was classified using unsupervised classification based on the Iterative Self Organizing Data Analysis Technique (ISODATA) algorithm. Twenty distinct categories were initially set; these were then aggregated and labelled as five categories: mixed vegetation, grasses, *Acacia auriculiformis*, bare soil, and water. The classified map was verified in the field and necessary corrections in misclassified areas were subsequently made. This means that the pixels belonging to the unidentified categories were extracted and reclassified. The newly classified pixels were then added back to the original image. To assess the accuracy of the classification, an error analysis was conducted comparing the classified image to an accurate ground truth map.

#### 3.2 Linear spectral unmixing

Linear spectral unmixing has often been implemented to deal with the problem of mixed pixels, and although theoretically imperfect because of the omission of the

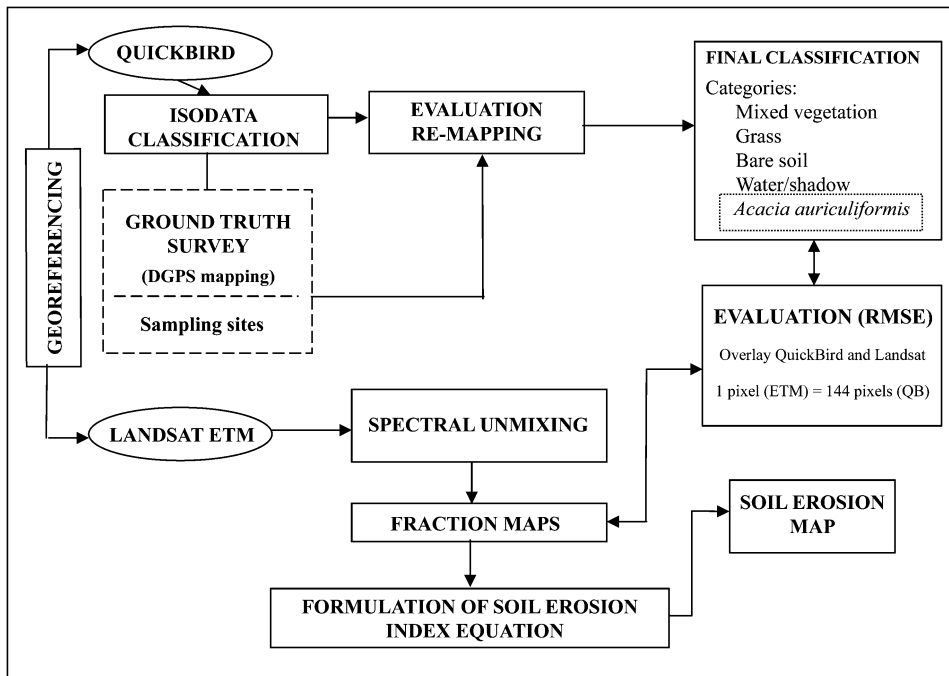


Figure 2. Flowchart of study procedure.

effect of multiple scattering between cover types (Roberts *et al.* 1993, Myneni *et al.* 1995), the errors associated with the linear assumptions have been found to be relatively minor (Kerdiles and Grondona 1995). An important assumption of LSU is that the spectral signature of a given pixel is the linear proportion-weighted combination of the end-member spectra (Smith *et al.* 1990). Mathematically, the LSU model is expressed as:

$$R_i = \sum_{j=1}^n f_j r_{ij} + \varepsilon_i \quad \text{and} \quad \sum_{j=1}^n f_j = 1; \quad 0 \leq f_j \leq 1 \quad (1)$$

where  $i$  is the number of spectral bands used;  $j=1, \dots, n$  is the number of end-members;  $R_i$  is the spectral reflectance of the mixed pixel in band  $i$ ;  $f_j$  is the fraction of the pixel area covered by the end-member  $j$ ;  $r_{ij}$  denotes the reflectance of the end-member  $j$  in band  $i$ ; and  $\varepsilon_i$  is the residual error in band  $i$ . In addition, for constrained spectral unmixing, two constraints were maintained in the solution of  $f_j$  values: the fractions across all end-members sum to one; and each end-member fraction is in the range 0 to 1. Input for the model is the spectral reflectance ( $R_i$ ) and the pure spectra of components in the pixel ( $r_{ij}$ ). Substituting these known parameters into the equation will give the areal proportion for end-members. A unique solution is possible as long as the number of end-members is equal to the number of spectral bands plus one. The residual error  $\varepsilon$  is the difference between the measured and modelled spectrum in each band. Residuals over all bands for each pixel in the image can be averaged to give an RMSE, which is useful in assessing the validity of selected end-members. For example, a high RMSE or high band residuals and negative or unrealistic fractions indicate a poor fit of the model and reveal inappropriate end-member selections.

It is well recognized that Landsat ETM data are hampered by the low spectral dimensionality and by low spatial resolution, which limits the selection of a few pure non-mixed pixels (Van der Meer and de Jong 2000). In a standard application of SMA, a fixed number of representative end-members, usually between two and five, are selected. However, this procedure is limited because the selected end-member spectra may not effectively model all elements in the image, or a pixel may be modelled by end-members that do not correspond to the materials located in its field of view. Both cases result in decreased accuracy of the estimated fractions (Sabol *et al.* 1992).

Several techniques have been used to select end-members from multispectral images (e.g. Adams *et al.* 1995, Tompkins *et al.* 1997, Painter *et al.* 1998, Oki *et al.* 2002, Small 2003, Wu and Murray 2003), including the use of principal component analysis (Maselli 1998), two-dimensional feature space plots (Peterson and Stow 2003) and identification of pure pixels with reference to field data (Shoshany and Svoray 2002). In this study, a combination of automatic and supervised end-member selection was performed on the Landsat ETM image. The minimum noise fraction (MNF) algorithm was applied to the reflectance image in which the MNF-transformed data were used as input to determine the most spectrally pure pixels (i.e. candidate end-members) in the image. MNF consists of essentially two cascaded principal component transformations that first compute the estimated noise covariance matrix to decorrelate and rescale the noise in the data and then perform a standard principal component transform of the noise whitened data (Garcia and Ustin 2001). In the MNF transform, the noise is separated from the data by using only the coherent portions, thus improving the spectral processing results. Previous

studies have shown that the use of the MNF transform can improve the quality of fraction images (Van der Meer and de Jong 2000) through decorrelation. Thus the MNF transform was used in this study. The pixel purity index (PPI) was used to find the most spectrally pure pixels in the image (Boardman *et al.* 1995). The PPI stipulates how many times the pixel is extreme in the simplex. The most spectrally pure pixels typically correspond to spectrally unique materials. Hence, the pixels with the highest PPI values were selected as candidate end-members as they are linearly independent in most dimensions. The final end-members were then selected by referring to QuickBird image data and actual field surveys (e.g. bare soils are mostly associated with dirt roads and cultivated areas, vegetations with homogeneous canopy). This was facilitated by using DGPS. One advantage of implementing MNF-PPI is that it separates purer pixels from more mixed ones, thus reducing the number of pixels to be analysed, which makes separation and identification of end-members more easily.

Five end-members were identified: mixed vegetation, grass, *Acacia auriculiformis*, bare soil, and water/shadow. The average reflectance of the selected representative pixels (average of 6–20 pixels) with high PPI values that corresponded to selected end-members were used in the unmixing process. The scatter plot of the mean reflectance values of the end-members is shown in figure 3.

The mixed vegetation areas are characterized by a mixture of different forest tree species, including mahogany (*Swietenia macrophylla*), narra (*Pterocarpus indicus*) and acacia (*Acacia mangium*), and very dense shrubs, herbs and bamboos that are found mostly along valleys and creeks. In the false colour composite (FCC) of the QuickBird image shown in figure 4, these are represented by a bright red colour, indicating the abundance of green vegetation. This is where most of the pixels with high PPI values for green vegetations were identified and therefore selected as end-members. The grass areas consist of both tall and creeping grasses and can be seen in the QuickBird image as a very light red colour. *Acacia auriculiformis* is represented as dark red in the FCC of QuickBird. This area is characterized by plantation trees of *Acacia auriculiformis*, as the name implies. *Acacia Auriculiformis* and grasses were

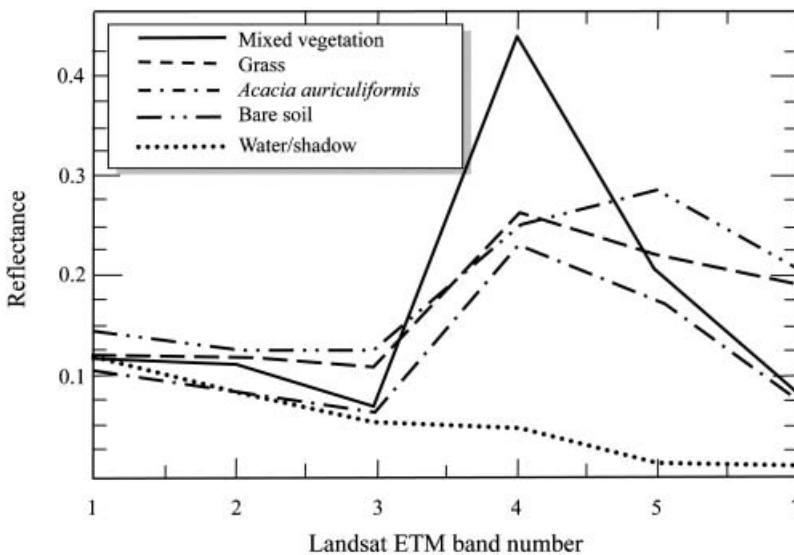


Figure 3. Spectral plot of selected end-members.

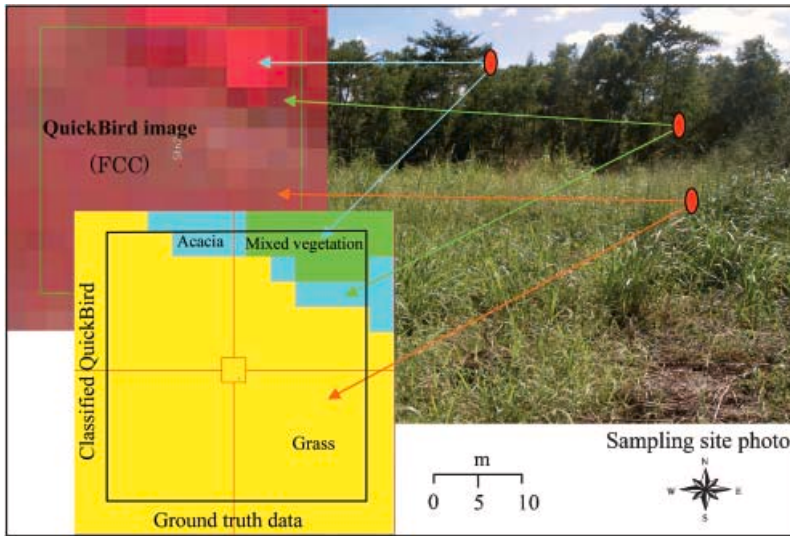


Figure 4. Sampling site and the process of registering the actual land cover into QuickBird imagery. Each sampling site has an area of about 900 m<sup>2</sup>.

selected as separate categories instead of combining them with mixed vegetation because the spectral reflectances of these are significantly different (figure 3). The bare soil end-member represents roads and cultivated lands. The image was taken during the last month of the dry season, and therefore had almost 100% exposed soil. The final end-member, shadow, accounts for variations in illumination caused by topography and surface textures, particularly of tree canopy. The shade end-member was selected from the water body because it is assumed that both have similar spectral characteristics (Bryant 1996). However, because shadow is not a physical component, it was removed by normalization (Smith *et al.* 1990, Hill *et al.* 1994, Adams *et al.* 1995). The fraction shadow/water ( $F_{\text{shadow}}$ ) was removed by rescaling each fraction image (except the shade fraction) with the normalization factor

$$f = 1 / (1 - F_{\text{shadow}}) \quad (2)$$

so that they sum again to one. This process removes shadow components from the image.

LSU was then performed on the Landsat ETM image using the different end-member spectra and end-member combinations. The unmixing was constrained to ensure that the fraction of any end-member lies between 0 and 1, and the sum of fractions for each pixel is equal to 1. The output of unmixing consisted of a proportion map of each selected end-member and an RMSE.

Initial residual analysis of each spectral band showed a high error for areas that were composed of *Acacia auriculiformis*, justifying the addition of an *Acacia auriculiformis* end-member.

### 3.3 Validation using very high-resolution image and field data

We used the classified QuickBird image to validate the accuracy of LSU. To make direct comparison, the QuickBird image was resampled to a pixel size of 2.5 m and

integrated to Landsat ETM resolution (30 m). Our goal was to match each pixel of Landsat ETM to its corresponding area in the QuickBird image (refer to figure 5). We assumed that the pixel size of 2.5 m represents the pure cover component (end-member); thus the total number of these pure pixels in a 30 × 30 m area gives the actual proportion of that end-member. As we have also field validated the classified QuickBird, we observed that the 2.5 m resolution is adequate to image the relevant land cover components and detect the presence of fairly small bare soil areas. The field validation also made it possible to assess the image-to-image registration. Visual comparison of the interactively overlaid images showed no evidence for systematic misregistration.

The LSU-RMSE was then computed for each land cover component. The classified QuickBird image was regarded here as the true coverage. Hence, the LSU-RMSE for all pixels that covers the whole overlapping area was computed as follows:

$$\text{LSU-RMSE} = \sqrt{\frac{\sum_{i=1}^n (a_i - a_q)^2}{n}} \quad (3)$$

where  $i$  is the number of land cover components;  $a_i$  is the fractional abundance of land cover components (end-members) in each pixel of the Landsat ETM image determined by unmixing;  $a_q$  is the ‘true fraction’ of the land cover component of the same type for the same pixel in the Landsat ETM image, measured from the QuickBird image; and  $n$  is the total number of Landsat ETM pixels used in the study.

There is, however, some uncertainty with the use of a very high resolution image to validate the results of the LSU. It should be noted that 100% orthorectification accuracy and image-to-image registration, even with the aid of differentially corrected GPS of any image, is practically impossible. We tried to co-register a 30 × 30 m against a 2.5 × 2.5 m resolution image and the smallest possible RMSE

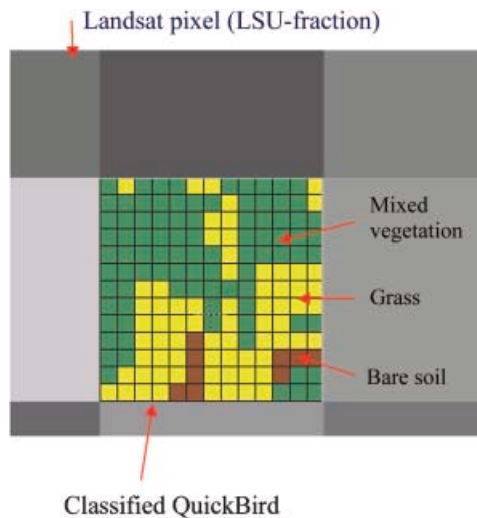


Figure 5. An illustrative example for validating the accuracy of LSU. The number of QuickBird pixels representing a given end-member within the 30 × 30 m (Landsat ETM resolution) gives the actual proportion of that end-member.

that we obtained was 0.21 Landsat ETM pixel. Although care was taken in the image-to-image registration process so as to minimize the RMSE, a small misregistration may be a significant source of error. As an example, an RMSE of 0.21 could translate to about 50 pixels locational errors per pixel of the Landsat ETM.

Therefore, to account for the uncertainty in the image registration, the LSU fractions were also compared with the actual land cover fractions measured from a classified QuickBird image at each sampling site location. In this method, we first identified a  $30 \times 30$  m area on the ground and marked its location on the QuickBird image (figure 4). This process makes it possible to further check the accuracy of the QuickBird classification and the validity of the 2.5 m pixel size to represent pure cover (end-member). The fractions of each land cover component were then determined from the classified QuickBird and compared to the LSU fractions. To account for the location error, as discussed earlier, the LSU fractions of each land cover component were taken from the average on the  $2 \times 2$  pixel window. Comparison between the QuickBird and Landsat data was performed using linear regression.

### 3.4 Delineation of potential erosion areas

Having determined the accuracy of the LSU, its applicability in delineating potential erosion areas was then evaluated. Two water-related factors that cause soil erosion are rainfall and run-off. Dense vegetation prevents these factors from breaking up soil particles and carrying them downslope. The above-ground cover absorbs the energy of falling raindrops, running water and wind, so that less is directed at the soil. The below-ground components, comprising the root system and plant residues, contribute to the mechanical strength of the soil and increase the surface roughness that slows down the surface run-off. Thus, as long as vegetation cover is unbroken, erosion is less likely despite the erosivity of the rainfall, slope steepness and soil instability. Without cover, the rainfall impact would detach soil particles and they would be carried out by running water. A review of studies on the relationship between soil erosion and vegetation abundance in a tropical environment indicated a significant increase in soil erosion with decreasing vegetation cover. For instance, Kellman (1969), using small plots to measure soil erosion under various vegetative covers in the Philippines, reported an exponential increase in annual soil loss with decreasing vegetative abundance. Similar trends were reported by Veracion (1980), Fauler and Heady (1981) and Laflen and Colvin (1981). Their general observation was that the greater the amount of vegetative cover, the lesser the soil erosion, whereas the more exposed soil or bare soil, the higher the soil erosion. Based on this concept, we used the fractional abundance of bare soil and vegetation abundance (as determined from the linear SMA) to define a bare soil/vegetation cover ratio as an indicator of susceptibility to soil erosion. The erosion index ( $E_i$ ) is defined as follows:

$$E_i = \frac{F_{bs}}{1 + F_{mv} + F_g + F_a} \quad (4)$$

where  $F_{bs}$ ,  $F_{mv}$ ,  $F_g$  and  $F_a$  are the fractions of bare soil, mixed vegetation, grass and *Acacia auriculiformis*, respectively. The equation assumes that soil erosion occurs only when there are exposed soils that are subject to soil detachment by raindrop impact and surface run-off. Additionally, it was assumed that in densely vegetated

areas, which could be either forest or grassland, soil erosion could be apparently equal to zero. One significant result from major soil erosion studies conducted in the Philippines indicated that a good grass cover is nearly as good as dense forest and just as good as, or even better than, secondary forest cover in protecting the soil from erosion (Kellman 1969, Bayotlang 1986, David 1988). Thus  $F_{mv}$ ,  $F_g$  and  $F_a$  can be combined with  $F_{veg}$  in the equation to represent all types of vegetation. The addition of 1.0 in the denominator limits the  $E_i$  value between 0 to 1, with higher values indicating more bare soil (high susceptibility to erosion) and low values corresponding to high vegetation (no soil erosion). An  $E_i$  map was generated using equation (4). The resulting map was interpreted and reclassified based on the observed actual soil erosion in each sampling site.

4. Results

The classified QuickBird image is shown in figure 6. The classification resulted in the following coverage: mixed vegetation, 17.1%; grass, 22.0%; *Acacia auriculiformis*, 53.4%; bare soil, 5.0%; and water/shadow, 2.5%. An overall accuracy of 98.8% and a kappa coefficient of 0.98 were obtained in the image classification (table 1). Excluding water/shadow, mixed vegetation had the highest classification accuracy with 99.7%, followed by bare soil with 99.2% accuracy. and *Acacia auriculiformis* and grass had 98.9% and 97.8% classification accuracy, respectively.

The accuracy of the LSU is summarized in table 2, which shows the LSU-RMSE for each land cover under four (mixed vegetation, grass, bare soil and water/shadow) and five (mixed vegetation, grass, *Acacia auriculiformis*, bare soil and water/shadow) end-member combinations. Also shown in the table is the total percentage coverage

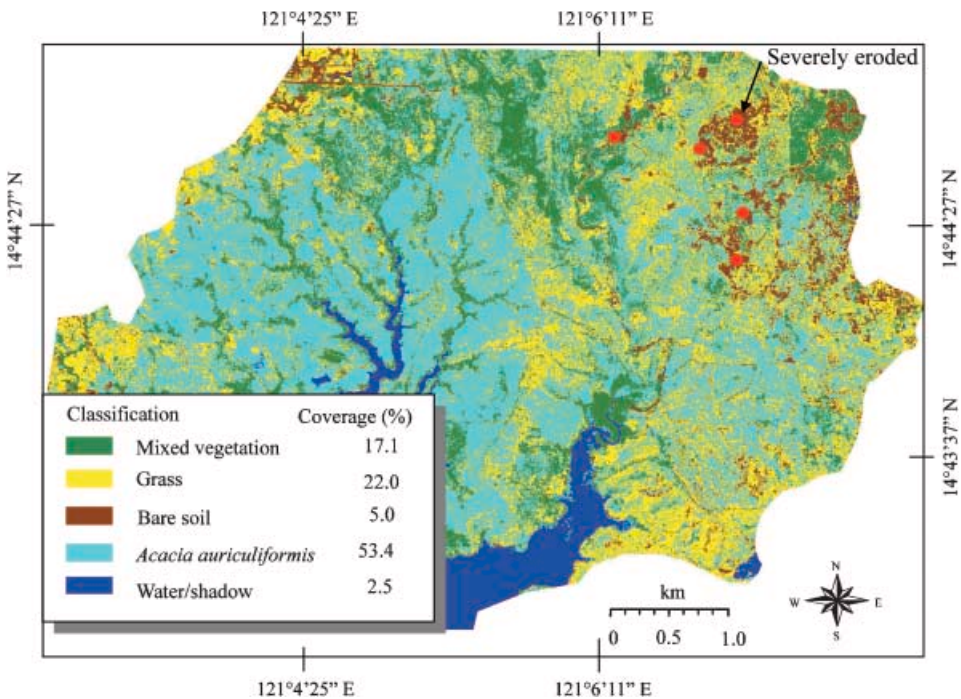


Figure 6. Classified QuickBird image using the ISODATA classification algorithm.

Table 1. Error matrix for the classified QuickBird image using ground truth data (%).

	Mixed vegetation	Grass	<i>Acacia auriculiformis</i>	Bare soil	Water/shadow
Mixed vegetation	99.7	0.0	0.4	0.0	0.0
Grass	0.2	97.8	0.7	0.8	0.0
<i>Acacia auriculiformis</i>	0.1	1.8	98.9	0.0	0.0
Bare soil	0.0	0.4	0.0	99.2	0.0
Water/shadow	0.0	0.0	0.0	0.0	100
Total	100	100	100	100	100

Overall accuracy: 98.8%.

Kappa coefficient: 0.98.

of each category as determined from the classified QuickBird image and from the different fraction images. Adding another end-member, *Acacia auriculiformis*, did improve the general fit as indicated by its relatively low LSU-RMSE. Moreover, the removal of shadow generated more accurate aerial estimates of the land cover component, matching more closely the measured area from QuickBird (table 2). The lowest LSU-RMSE was obtained in bare soil (8.7%), followed by mixed vegetation (10.0%). The *Acacia auriculiformis* and grass had LSU-RMSEs of 16.5% and 19.6%, respectively.

Figure 7 shows the normalized fraction images of mixed vegetation, grass, *Acacia auriculiformis* and bare soil, and the resulting RMSE image derived from the unmixed Landsat ETM. The high abundance of each end-member is indicated by bright pixels and the low abundance by darker pixels. Visual examination of the QuickBird image and the fraction images shows good correspondence for mixed vegetation, *Acacia auriculiformis* and bare soil. The spatial distribution of these three end-members generally agrees with the distribution in the QuickBird image. For example, the mixed vegetation is clearly distinguishable along creeks and the mid-upper and lower portions of the image. *Acacia auriculiformis*, which covers more than half of the study area, is clearly identifiable and highly concentrated in the south-western portion of the area. The bare soils are also distinctly clear (in the

Table 2. Linear spectral unmixing root mean square error (LSU-RMSE) from the comparison between the fractional abundance of land cover component derived from the LSU and measured from the QuickBird image.

Land cover	Four-end-member			Five-end-member			With shadow normalization		
	Cover (%)		LSU-RMSE (%)	Cover (%)		LSU-RMSE (%)	Cover (%)		LSU-RMSE (%)
	ETM	QB		ETM	QB		ETM	QB	
Mixed vegetation	48.8	70.5	33.0	12.3	17.1	13.0	19.3	17.1	10.0
Grass	45.8	22.0	20.3	31.1	22.0	20.1	29.5	22.0	19.6
<i>Acacia auriculiformis</i>	–	–	–	39.1	53.4	24.8	45.1	53.4	16.5
Bare soil	1.4	5.0	18.5	7.5	5.0	10.5	6.1	5.0	8.7
Water/shadow	15.8	2.5	13.7	10.0	2.5	8.8	–	(2.5)	–

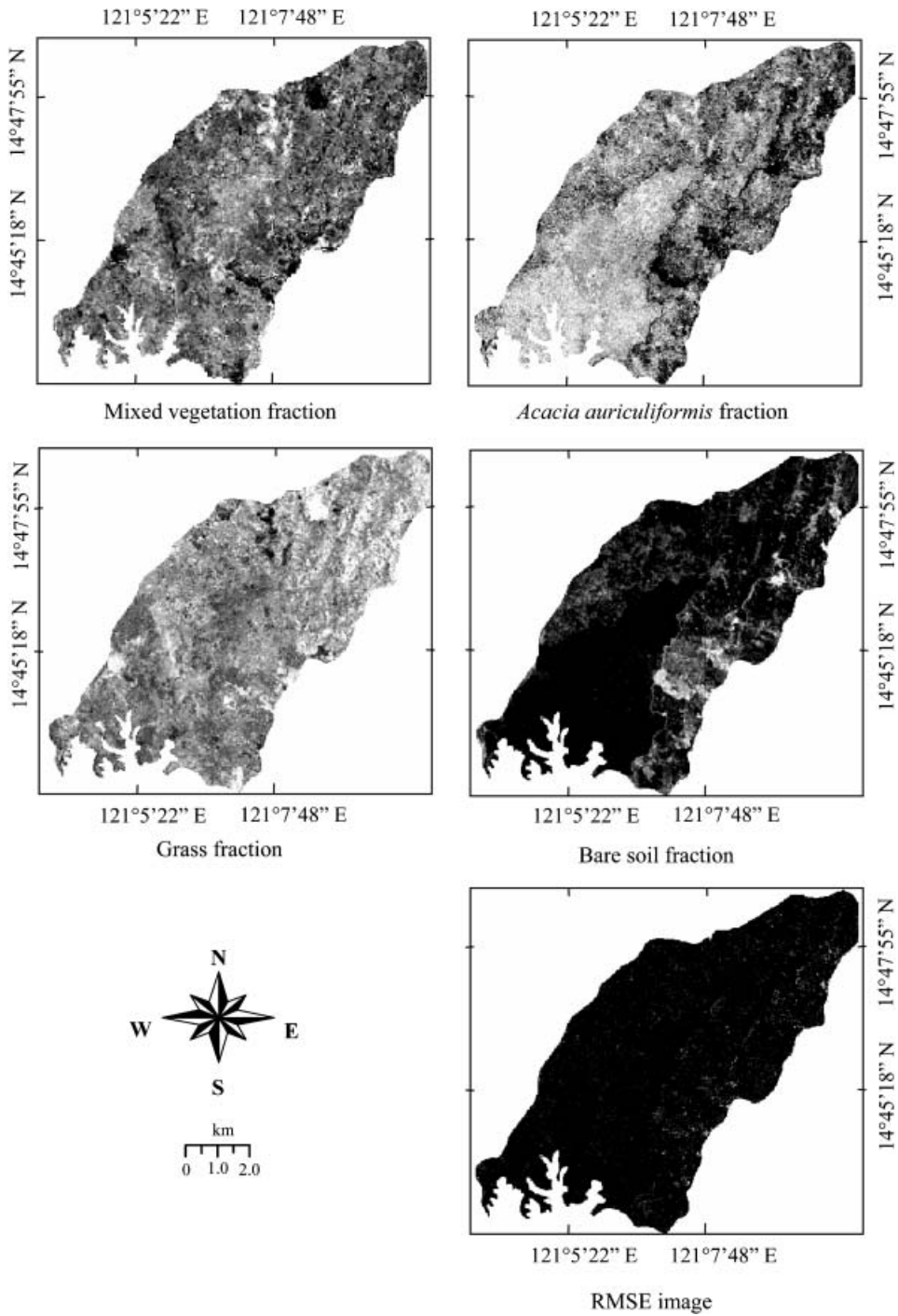


Figure 7. Normalized fraction and RMSE for the Landsat ETM four-end-member (mixed vegetation, grass, *Acacia auriculiformis* and bare soil) linear mixture model. The lighter the colour, the higher the proportion of end-member (and error) within the pixel.

bare soil fraction), appearing in isolated areas, whereas the grass end-member has no specific location and is scattered throughout the image. The RMSE image, representing the error between the original, mixed spectrum and the best-fit spectrum computed from the resulting end-member abundances, shows low spatial correlation (no recognizable pattern). The spatial distribution of the RMSEs shows that relatively higher values (RMSE=0.09–0.13 reflectance units) can be noted in areas of bare soils and grassland, and lower values in vegetation areas (mixed vegetation and *Acacia auriculiformis*). The high RMSE values in bare soil areas may be due to the fact that the representative pixels are to some extent combined with non-photosynthetic materials such as stones and litter. However, the overall average RMSE for the whole image is still small (=0.06), thus it can be deduced that the selected end-members were valid and sufficient. The low RMSE value, however, does not guarantee that the fraction estimates are accurate. Field validation is necessary to determine the accuracy of the end-member estimates.

Figure 8 presents a direct comparison between actual land cover fractions (measured from classified QuickBird) and LSU fractions. The results showed a significant correlation. This is especially true for mixed vegetation and *Acacia auriculiformis*, with correlation coefficients of 0.93 and 0.92, respectively. The correlation coefficient for grass is 0.88, and 0.86 for bare soil.

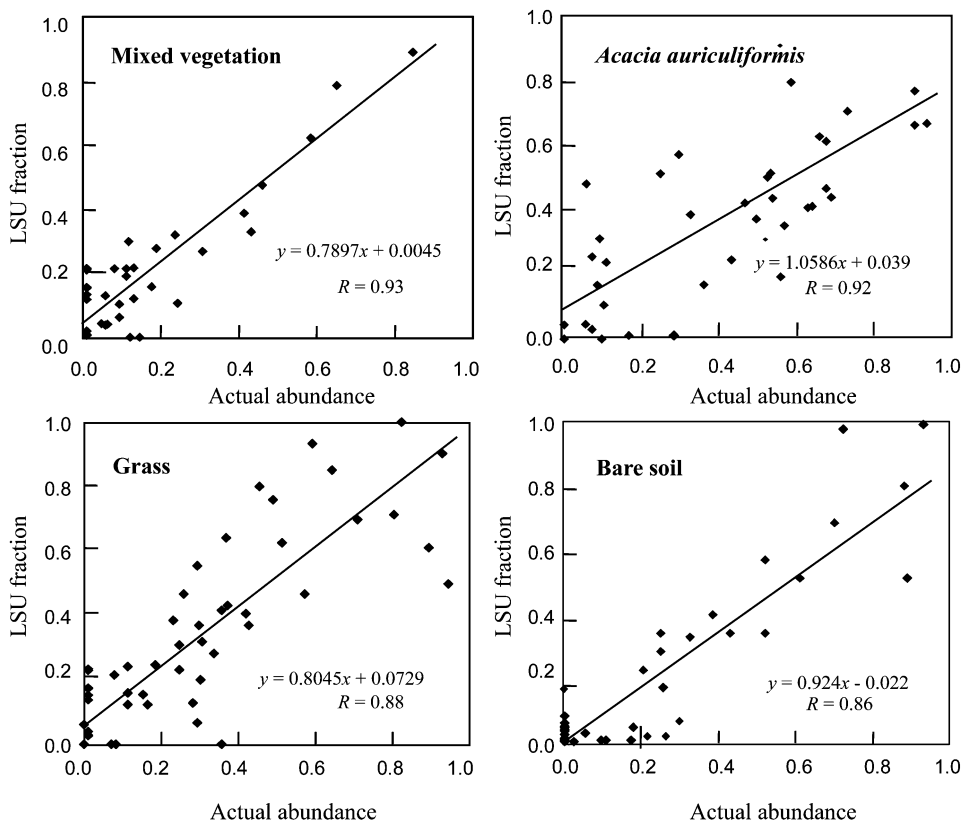


Figure 8. Comparison between ground cover abundance (measured from QuickBird) and LSU fraction.

The geographic locations of some of the areas noted with severe erosion during the fieldwork are indicated in the classified QuickBird image as dots shown in figure 6. Severe soil erosion is clearly visible because of the presence of deep channels/gullies and the exposure of subsurface soil. By contrast, no erosion was noted in the mixed vegetation area. Figure 9 shows the erosion index ( $E_i$ ) map derived from equation (4) using the normalized LSU fraction as input. Comparing this with the QuickBird image and ground data shows that the whiter pixels strongly correlate to the cultivated fields and bare soil areas, which were noted for severe erosion. The darker pixels, by contrast, match up with the mixed vegetation in the QuickBird image having no erosion observed.

A plot of soil erosion level at each sampling site (determined during the field work) and the estimated  $E_i$  value taken from the  $E_i$  map is shown in figure 10. An examination of the figure reveals some important relationships. For instance, by reclassifying the  $E_i$  map (figure 9) based on the erosion level (i.e. labelling those pixels with values ranging from 0.00 to 0.06 to erosion level 1), the densely mixed vegetation areas or those with no soil erosion were delineated. Likewise, by reclassifying pixels ranging from 0.06 to 0.40 to soil erosion level 2, moderate erosion areas were identified. Further classifying the  $E_i$  map indicates that it is possible to identify those areas noted with severe erosion ( $E_i$  value=0.80–1.0) and high erosion ( $E_i$  value=0.40–0.80). Figure 11 shows the soil erosion level for the

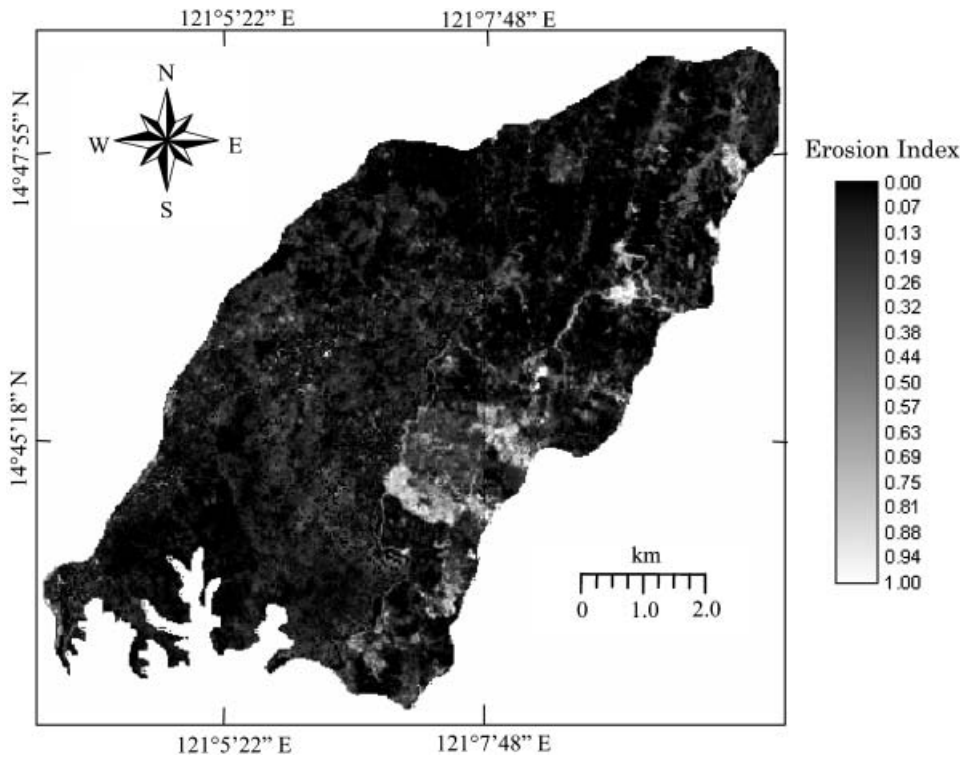


Figure 9. Erosion index map derived using equation (4). The values range from 0 (darker pixels) to 1 (lighter pixels). Lighter pixels indicate high erosion and darker pixels indicate low soil erosion.

Downloaded By: [University of Tokyo/TOKYO DAIGAKU] At: 05:34 20 August 2008

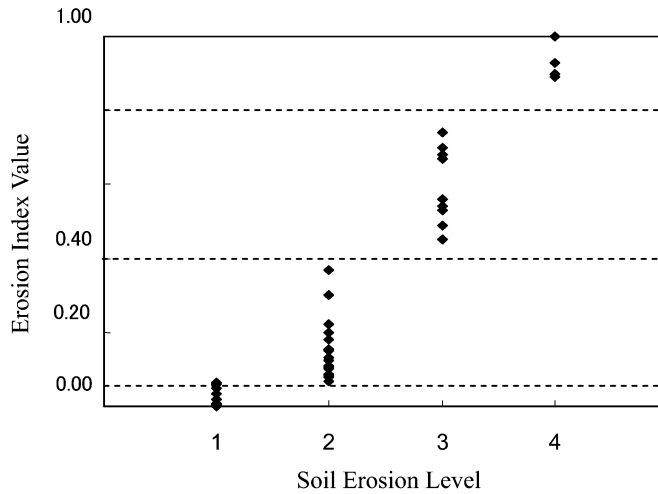


Figure 10. Soil erosion level at each sampling site and erosion index ( $E_i$ ) values. The  $E_i$  values at each sampling site were determined from the  $E_i$  map. Soil erosion levels 4, 3, 2 and 1 correspond to severe erosion, high erosion, moderate erosion and no erosion, respectively.

whole Lamesa watershed after the derivation of the  $E_i$  map using equation (4) and classification as described above. It shows that about 106 ha are severely eroded and about 498 ha are highly eroded (figure 11).

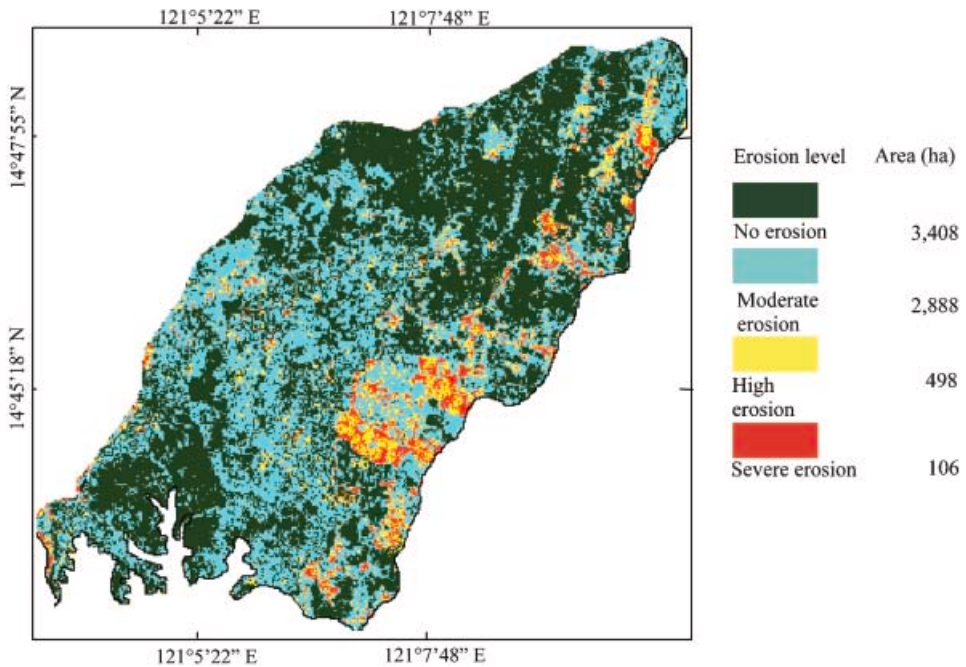


Figure 11. Soil erosion map (reclassified  $E_i$ ) for the whole study area. The four levels of soil erosion categorized based on field assessment of erosion level were: severe erosion (soil erosion level 4,  $E_i$  value=0.80–1.0), high erosion (soil erosion level 3,  $E_i$  value=0.40–0.80), moderate erosion (soil erosion level 2,  $E_i$  value=0.06–0.40) and no erosion (soil erosion level 1,  $E_i$  value=0.0–0.06).

## 5. Discussion

The tests for accuracy and applicability of LSU in mapping potential erosion areas in a tropical watershed were undertaken using high-resolution QuickBird image and ground truth data. In most of the previous studies on spectral unmixing, the commonly used method is through evaluation of the mathematical validity of the model using the RMSE, the root mean square of the difference between the observed and modelled reflectance of a given pixel. Although the RMSE method is simple and straightforward, it does not guarantee that the end-member abundance will agree with the actual land cover abundance (Small 2003). Other methods using ground reference data, such as those proposed by Elmore *et al.* (2000), are very labour intensive and cannot be regarded as producing an absolute reference against which the accuracy of land cover estimates could be judged. This is because of the difficulty of accurately linking field measurements to individual image pixels (Kuemmerle *et al.* 2006). Even with the use of the GPS, it is still difficult to identify the location of the four corners of a pixel and determine the percentage distribution of different land cover types within that pixel. In addition, the time gap between field measurements and the acquisition of the satellite image may incur further errors in validation because of the difference in environmental conditions during ground data collection and satellite acquisition (Myint 2006).

Using QuickBird as a substitute for ground measurements appears to be a valuable option for complementing ground-based methods. The very high spatial resolution of QuickBird permits the identification of different land covers, which makes it possible to compare the abundance estimates of different land covers on a wider scale. The almost simultaneous acquisition of QuickBird and Landsat ETM images, as conducted in this study, means that there are no substantial changes in the environmental conditions in the area that could contribute to the temporal error or inaccuracy of comparison. Great care, however, must be taken in using a very high-resolution image to validate the results of unmixing on a pixel-by-pixel basis because of geometric registration errors; a small mismatch in the registration can lead to significant errors. Currently, there are limits to geolocation accuracy for existing fine and coarse spatial resolution satellites because of different view angles and terrain variations, and because fine and coarse image sensors orbit different platforms.

Previous studies (Metternicht and Fermont 1998, Koch 2000, Haboudane *et al.* 2002) on the application of the spectral unmixing technique have shown its potential in the identification and mapping of degraded areas due to soil erosion. Most of these researches were applied in semi-arid environments where the reflective differences between the green vegetation, soil background, and shadow are unique and distinguishable. The remotely sensed data in these regions are largely influenced by soils and rocks (de Jong *et al.* 1999, Haboudane *et al.* 2002). Homogeneous green vegetation is rarely dominating and its cover is usually sparse. Hence, the analysis of soil erosion is usually based on the description of spectra as dictated by soil properties such as level of organic matter, iron oxides, clay minerals and carbonates (Hill *et al.* 1994, Metternicht and Fermont 1998, Koch 2000, Haboudane *et al.* 2002).

In tropical areas, however, the dominant covers found are various types of vegetation. Unlike in arid and semi-arid environments, large bare soil areas are uncommon and tend to be in patches (whose size is usually less than the dimensions of a pixel) randomly distributed over the watershed. The challenge in a tropical

environment is to be able to identify these bare soil areas and discriminate the various levels of vegetation abundance as these are the important indicators from which soil erosion susceptibility can be derived. Various approaches have been proposed to detect potential erosion areas, including direct visual interpretation, image classification and spectral indices, but because these methods rely on the pixel as the smallest quantity, the true abundance of the surface materials is not represented. The use of LSU is seen to be more appropriate because of its ability to identify bare soil areas and estimate vegetation abundance, which are not possible using simple image classification.

The soil erosion ( $E_i$ ) map obtained in this study is useful for evaluating soil erosion susceptibility of an area for soil conservation planning. For example, if a pixel representing an area has an  $E_i$  value of 0.8, this would suggest that the area has a higher susceptibility to soil erosion than an area with an  $E_i$  value of, for example, 0.4. Vrielig (2006) indicated that, for conservation prioritization, erosion rates are often not required but are merely indications of the spatial distribution of soil erosion.

In this study, the data used were obtained during the dry season (the summer of 2004). Having multirate remote sensing data to represent both dry and wet seasons may provide a general characterization of the area for the whole year. However, for the purpose of determining the susceptibility to erosion, the use of one image is sufficient. For example, this study used the Landsat ETM image taken in April, the last month of the dry season, because it gives the optimal condition by which susceptible erosion areas, especially bare soil areas, can be detected. Most of the grasses have dried up and soils are exposed. This has important implications considering that high erosion rates are likely to occur in barely vegetated areas once the rainy season comes. The method as described in this study thus offers a simple solution for detecting and monitoring areas susceptible to soil erosion.

## 6. Conclusions

The use of the spectral unmixing technique applied to Landsat ETM data offers an opportunity for better assessment of land conditions related to soil erosion in tropical watersheds. This study has shown that with proper use of the technique, especially on the selection of end-members, good quality fraction images can be obtained and subsequently used for detecting potential erosion areas. The incorporation of other ancillary data such as DEM in the results of the unmixing can provide quantitative information on the rate of soil erosion. However, for the purpose of this study, a qualitative evaluation is sufficient to determine the spatial distribution of crucial areas that need the utmost attention. Nevertheless, it is worth mentioning that the results can be used further as input for soil erosion modelling. Application of these methods in other areas should be conducted to determine whether the same classification scheme could be used in delineating the same erosion classes described in this study.

In the Philippines, where economic considerations are important, using a cheaper image for watershed management purposes is indispensable. Many large watershed areas are now threatened because of social and technical factors. Appropriate technologies that are useful and economical are needed to prevent further degradation of these watersheds. The high-resolution images such as those of QuickBird can be very useful but the high cost of these images dictates that it is not appropriate for application in large watersheds for most developing countries, such

as the Philippines. The use of an inexpensive image such as Landsat ETM along with the method presented in this paper is thus seen as a good alternative.

### Acknowledgements

We thank Marlo Mendoza, Valerio Mendoza, Glenn Paul Flores and Nemuel de Asis for their invaluable assistance during the initial data collection and fieldwork for this study. Our sincere gratitude is also accorded to the Hitachi Scholarship Foundation, Inc. (Japan) for extending financial support in the conduct of this study.

### References

- ADAMS, J.B., SABOL, D.E., KAPOS, V., FILHO, R.A., ROBERTS, D.A., SMITH, M.O. and GILLESPIE, A.R., 1995, Classification of multispectral images based on fractions of end-members: application to land-cover change in the Brazilian Amazon. *Remote Sensing of Environment*, **52**, pp. 137–154.
- ADAMS, J.B., SMITH, M.O. and JOHNSON, P.E., 1986, Spectral mixture modeling: a new analysis of rock and soil types at the Viking Lander 1 Site. *Journal of Geophysical Research*, **91**, pp. 8098–8112.
- BAYOTLANG, E.L., 1986, Evaluation of erosivity, erodibility and crop management factors of the Universal Soil Loss Equation. PhD dissertation, University of the Philippines Los Banos, Laguna, Philippines.
- BOARDMAN, J.W., KRUSE, F.A. and GREEN, R.O., 1995, Mapping target signatures via partial unmixing of AVIRIS data. In *Summaries of the Fifth Annual JPL Airborne Geoscience Workshop*, Vol. 1, pp. 23–26, Purdue University: JPL Publications 95-1.
- BOCCO, G., PALCIO, J.L. and VALENZUELA, C.R., 1991, Gully erosion modeling using GIS and geomorphological knowledge. *ITC Journal*, **3**, pp. 253–261.
- BOCCO, G. and VALENZUELA, C.R., 1988, Integration of GIS and image processing in soil erosion studies using ILWIS. *ITC Journal*, **4**, pp. 309–319.
- BRAYANT, R.G., 1996, Validated linear modeling of Landsat TM data for mapping evaporite minerals on a playa surface: methods and applications. *International Journal of Remote Sensing*, **17**, pp. 315–330.
- DAVID, W.P., 1988, Soil and water conservation planning: policy issues and recommendations. *Journal of Philippine Development*, **15**, pp. 47–84.
- DE JONG, S.M., PARACCHINI, M.L., BERTOLO, F., FOLVING, S., MEGER, J. and DE ROO, A.P.J., 1999, Regional assessment of soil erosion using the distributed model SEMMED and remotely sensed data. *Catena*, **37**, pp. 291–308.
- DWIVEDI, R.S., SANKAR, T.R., VENKATARATNAM, L., KARALE, R.L., GAWANDE, K.V., SESHAGIRI, K.V., SENCHAUDHARY, S., BHAUMIK, K.R. and MUKHARJEE, K.K., 1997, The inventory and monitoring of eroded lands using remote sensing data. *International Journal of Remote Sensing*, **18**, pp. 107–119.
- ELMORE, A.J., MUSTARD, J.F., MANNING, S.J. and LOBELL, D.B., 2000, Quantifying vegetation change in semi-arid environment: precision and accuracy of spectral mixture analysis and the Normalized Difference Vegetation Index. *Remote Sensing of Environment*, **73**, pp. 87–102.
- EUGENIO, F. and MARQUEZ, F., 2003, Automatic satellite image georeferencing using a contour-matching approach. *IEEE Transactions on Geoscience and Remote Sensing*, **41**, pp. 2869–2880.
- FAULER, J.M. and HEADY, 1981, Suspended sediment load production potential on undisturbed forest land. *Journal of Soil Conservation*, **36**, pp. 18–23.
- FLORAS, S.A. and SGOURAS, I.D., 1999, Use of geoinformation techniques in identifying and mapping areas of erosion in a hilly landscape of central Greece. *International Journal of Applied Earth Observation and Geoinformation*, **1**, pp. 68–77.

- FULAJTAR, E., 2001, Identification of severely eroded soils from remote sensing data tested in Risnovce. In *Sustaining the Global Farm*, D.E. Stott, R.H. and G.C. Steinhardt (Eds), pp. 1075–1081, Purdue University and USDA-ARS.
- GARCIA, M. and USTIN, S.L., 2001, Detection of interannual vegetation responses to climatic variability using AVIRIS data in a coastal savanna in California. *IEEE Transactions on Geoscience and Remote Sensing*, **39**, pp. 1480–1490.
- HABOUDANE, D., BONN, F., ROYER, A., SOMMER, S. and MEHL, W., 2002, Land degradation and erosion risk mapping by fusion of spectrally-based information and digital geomorphometric attributes. *International Journal of Remote Sensing*, **23**, pp. 3795–3820.
- HILL, J., MEHL, W. and ALTHERR, M., 1994, Land degradation and soil erosion mapping in Mediterranean ecosystems. In *Imaging Spectrometry: A Tool for Environment Observations*, J. Hill and H. Megier (Eds), pp. 237–260 (Dordrecht: Kluwer Academic Publishers).
- KELLMAN, M.C., 1969, Some environmental components of shifting cultivation in Upland Mindanao. *Journal of Tropical Geography*, **28**, pp. 1–28.
- KERDILES, H. and GRODONA, M.O., 1995, NOAA-AVHRR NDVI decomposition and subpixel classification using linear mixing in the Argentinean Pampa. *International Journal of Remote Sensing*, **16**, pp. 1303–1325.
- KOCH, M., 2000, Geological controls of land degradation as detected by remote sensing: a case study in Los Monegros, north-east Spain. *International Journal of Remote Sensing*, **21**, pp. 457–473.
- KUEMMERLE, T., RÖDER, A. and HILL, J., 2006, Separating grassland and shrub vegetation by multivariate pixel-adaptive spectral mixture analysis. *International Journal of Remote Sensing*, **27**, pp. 3251–3271.
- KUMAR, A.B., DWIVEDI, R.S. and TIWARI, K.N., 1996, The effects of image scale on delineation of eroded lands using remote sensing data. *International Journal of Remote Sensing*, **17**, pp. 2135–2143.
- LAFLEN, J.M. and COLVIN, T.S., 1981, Effects of crop residue on soil loss from continuous row cropping. *Transactions of the American Society of Agricultural Engineers*, **24**, pp. 605–609.
- MASELLI, F., 1998, Multiclass spectral decomposition of remotely sensed scenes by selective pixel unmixing. *IEEE Transactions on Geoscience and Remote Sensing*, **36**, pp. 1809–1820.
- METTERNICHT, G.I. and FERMONT, A., 1998, Estimating erosion surface features by linear mixture modeling. *Remote Sensing of Environment*, **64**, pp. 254–265.
- METTERNICHT, G.I. and ZINCK, J.A., 1998, Evaluating the information content of JERS-1 SAR and Landsat TM data for discrimination of soil erosion features. *ISPRS Journal of Photogrammetry and Remote Sensing*, **53**, pp. 143–153.
- MYINT, S.W., 2006, Urban vegetation mapping using sub-pixel analysis and expert system rules: a critical approach. *International Journal of Remote Sensing*, **27**, pp. 2645–2665.
- MYNENI, R.B., MAGGION, S., JAQUINTA, J., PRIVETTE, J.L., GORDON, N., PINTY, B., KIMES, D.S., VERSTRAETE, M.M. and WILLIAMS, D.L., 1995, Optical remote sensing of vegetation: modeling, caveats, and algorithms. *Remote Sensing of Environment*, **51**, pp. 169–188.
- OKI, K., OGUMA, H. and SUGITA, M., 2002, Subpixel classification of alder trees using multitemporal Landsat Thematic Mapper imagery. *Photogrammetric Engineering and Remote Sensing*, **68**, pp. 77–82.
- PAINTER, T.H., ROBERTS, D.A., GREEN, R.O. and DOZIER, J., 1998, The effect of grain size on spectral mixture analysis of snow-covered area from AVIRIS data. *Remote Sensing of Environment*, **65**, pp. 320–332.
- PETERSON, S.H. and STOW, D.A., 2003, Using multiple image end-member spectral mixture analysis to study chaparral regrowth in southern California. *International Journal of Remote Sensing*, **24**, pp. 4481–4504.

- ROBERTS, D.A., SMITH, M.O. and ADAMS, J.B., 1993, Green vegetation, non-photosynthetic vegetation, and soils in AVHRRIS data. *Remote Sensing of Environment*, **44**, pp. 255–269.
- SABOL, D.E., ADAMS, J.B. and SMITH, M.O., 1992, Quantitative sub-pixel spectral detection of targets in multispectral images. *Journal of Geophysical Research*, **97**, pp. 2659–2672.
- SERVENAY, A. and PRAT, C., 2003, Erosion extension of inundated volcanic soils of Mexico by aerial photographs and remote sensing analysis. *Geoderma*, **117**, pp. 367–375.
- SETTLE, J.J. and DRAKE, N.A., 1993, Linear mixing and the estimation of ground cover proportions. *International Journal of Remote Sensing*, **14**, pp. 1159–1177.
- SHOSHANY, M. and SVORAY, T., 2002, Multidate adaptive unmixing and its application to analysis of ecosystem transitions along a climatic gradient. *Remote Sensing of Environment*, **82**, pp. 5–20.
- SMALL, C., 2001, Estimation of urban vegetation abundance by spectral mixture analysis. *International Journal of Remote Sensing*, **22**, pp. 1305–1334.
- SMALL, C., 2003, High spatial resolution spectral mixture analysis of urban reflectance. *Remote Sensing of Environment*, **88**, pp. 170–186.
- SMITH, M.O., JOHNSON, P.E., ADAMS, J.B. and GILLESPIE, A.R., 1990, Vegetation in deserts: I. A regional measure of abundance from multispectral images. *Remote Sensing of Environment*, **31**, pp. 1–26.
- TOMPKINS, S., MUSRAD, J.F., PIETERS, C.M. and FORSYTH, D.W., 1997, Optimization of end-members for spectral mixture analysis. *Remote Sensing of Environment*, **59**, pp. 472–489.
- VAN DER MEER, F., 1995, Spectral unmixing of Landsat Thematic Mapper data. *International Journal of Remote Sensing*, **16**, pp. 3189–3194.
- VAN DER MEER, F. and DE JONG, S.M., 2000, Improving the results of spectral unmixing of Landsat Thematic Mapper imagery by enhancing the orthogonality of end-members. *International Journal of Remote Sensing*, **21**, pp. 2781–2797.
- VERACION, V.R., 1980, Effects of some land uses and cover types on surface run-off and soil loss in the Ambuklao watershed. Forest Research Institute Report. College Laguna, Philippines.
- VRIELING, A., 2006, Satellite remote sensing for water erosion assessment: a review. *Catena*, **65**, pp. 2–18.
- WU, C. and MURRAY, A.T., 2003, Estimating impervious surface distribution by spectral mixture analysis. *Remote Sensing of Environment*, **84**, pp. 493–505.